Fluid Structure Interaction Modeling of an Artificial Heart Membrane Test Bench

Alex Sanaei[1], Nicolas Van Dorsselaer[1], Charlotte Toureng[2], Yannick Tarnowski[2], Loic Mées[3], Nathalie Grosjean[3]

[1]Dynas+, 5 avenue Didier Daurat 31400 Toulouse France

[2]CARMAT, 36, avenue de l'Europe Immeuble l'Etendard 78140 Vélizy-Villacoublay, France

[3]CNRS, Ecole Centrale de Lyon, INSA Lyon, Université Claude Bernard Lyon 1, LMFA, UMR5509, 36 Avenue Guy de Collongue 69134 Ecully, France

1 Introduction

Fluid–structure interaction (FSI) plays a central role in the design and validation of cardiovascular devices, particularly total artificial hearts, where compliant membranes dynamically interact with pulsatile flows under physiological conditions. In such systems, accurately predicting the coupled behavior of fluids and deformable structures is essential for optimizing performance, minimizing blood damage, and ensuring long-term biocompatibility. While computational approaches offer powerful tools for exploring these complex interactions, their predictive value strongly depends on the integration of high-quality experimental data.

In this context, the Laboratoire de Mécanique des Fluides et d'Acoustique of Lyon, France (LMFA) and CARMAT initiated a detailed experimental campaign to characterize the behavior of the hyperelastic membrane that constitutes the interface between hydraulic actuation and the blood compartment in CARMAT's total artificial heart. This membrane is subjected to large deformations and interacts with highly unsteady internal flows, making it a critical component for both mechanical efficiency and hemocompatibility. Using advanced optical diagnostics — including Particle Image Velocimetry (PIV) and Particle Tracking Velocimetry (PTV) — the LMFA quantified membrane kinematics and surrounding flow velocity fields under representative operating conditions.

To complement these experiments, a high-fidelity FSI model was developed using DEP Meshworks and Ansys LS-DYNA by Dynas+, coupling incompressible fluid dynamics (ICFD solver) with large-deformation hyperelastic solid mechanics. This numerical framework was calibrated against the LMFA data to ensure realistic reproduction of the membrane's dynamic response.

2 LMFA's Experimental setup

The test bench developed by LMFA is shown in Fig.1:

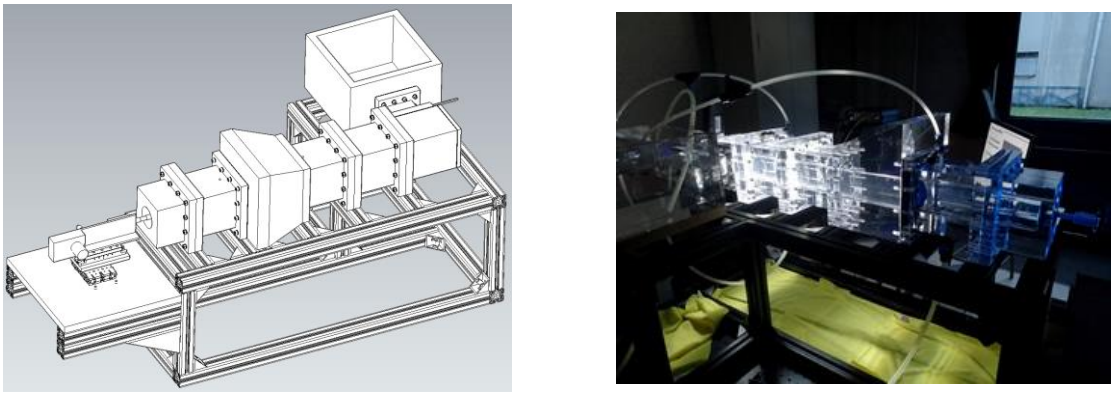

Fig.1: CAO of the test bench (left) and picture of the test bench (right). Source: LMFA's report [1]

It consists of a tank filled with 110 mm of water (1), several blocks that create a flow path for the fluid (2), the hyperelastic membrane used in CARMAT total artificial heart (3) and a piston-driven system used to initiate fluid movement (4). The entire experimental test bench is built on an assembly of aluminum profiles (5).

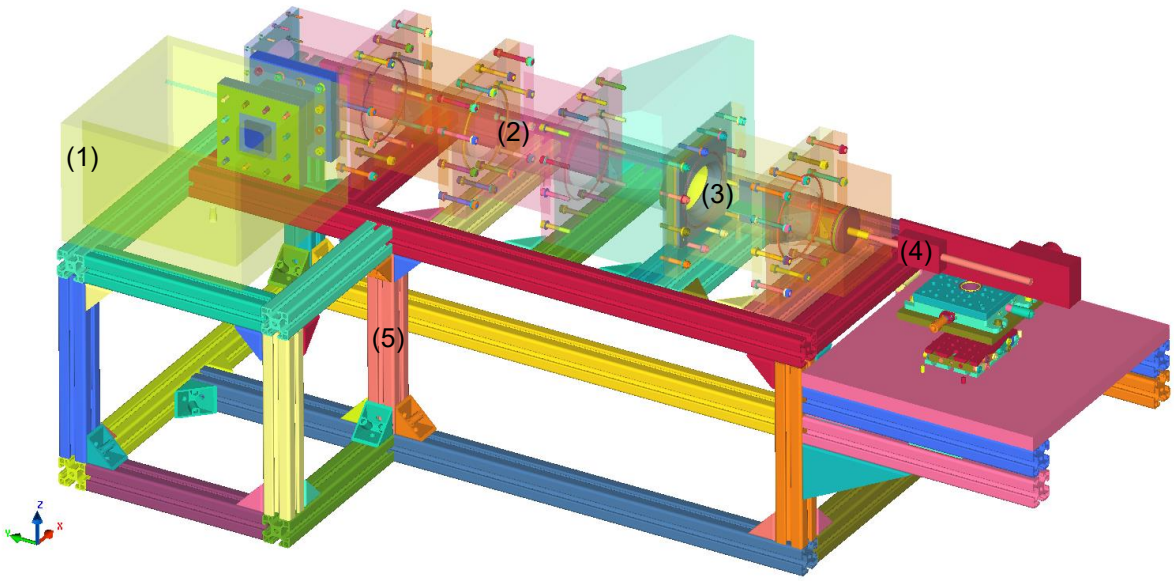

Fig.2: CAO of the test bench (transparency activated, view from the side).

Here is another view of the CAO model:

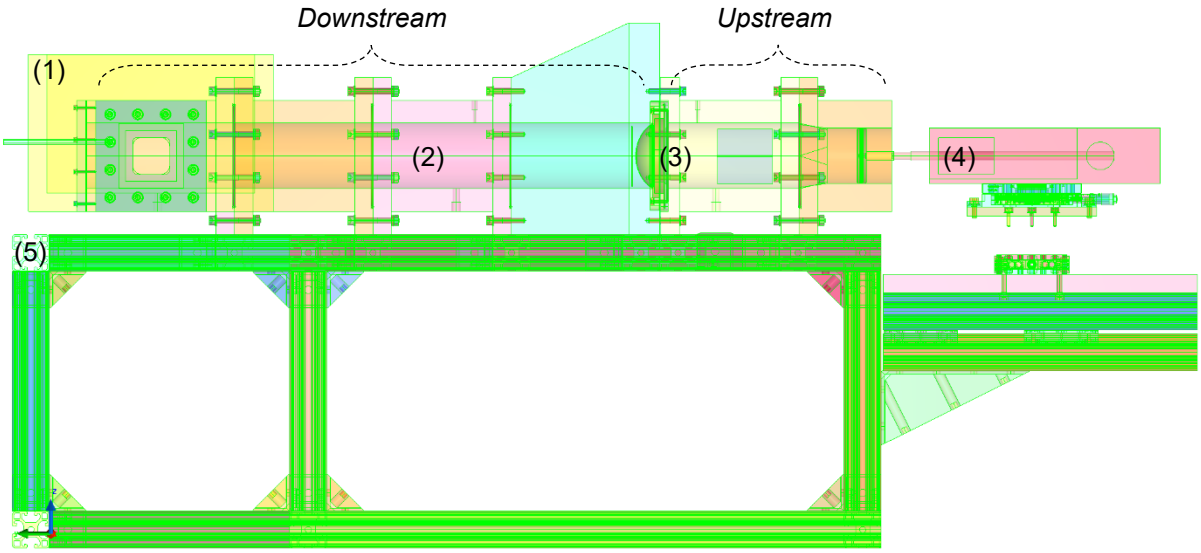

Fig.3: CAO of the test bench (transparency activated, isometric view)

The straight channel has an elliptical cross-section, designed to match the shape of the membrane. Water is present both upstream and downstream of the membrane. The deformation of the membrane is driven by the motion of a piston located upstream, which in turn generates a fluid flow downstream that is to be characterized. In this study, a polymer membrane with hyperelastic behavior is used—without any hybrid structure or bovine pericardium overlay.

The hyperelastic membrane (3) is shown below:

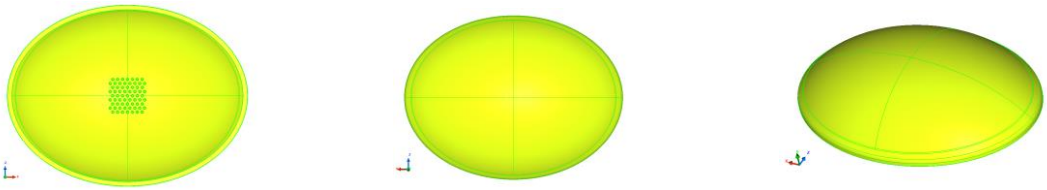

Fig.4: CAO views of the hyperelastic membrane

Here are the relevant dimensions of the membrane:

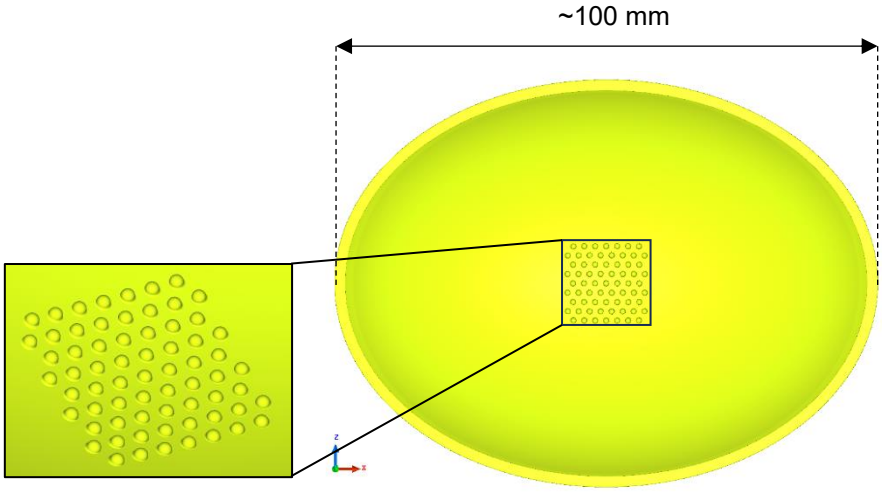

Fig.5: The hyperelastic membrane with its microspheres

The test bench is equipped with several measurement systems to comprehensively characterize the flow and membrane behavior. A distance sensor monitors the piston displacement, while two pressure sensors are positioned upstream and downstream of the membrane to capture pressure variations. A Particle Image Velocimetry (PIV) system is used to measure the velocity field in the flow, and a four-camera setup, coupled with dedicated tracking software, enables membrane deformation tracking via the PTV-4D (Particle Tracking Velocimetry) technique. For this purpose, white markers were painted on the membrane surface and tracked by the PTV-4D system, yielding numerous particle trajectories and snapshots that allow for the reconstruction of the membrane's instantaneous 3D shape. PIV measurements were performed in vertical and horizontal planes downstream of the membrane, as well as in a vertical plane upstream of it [1].

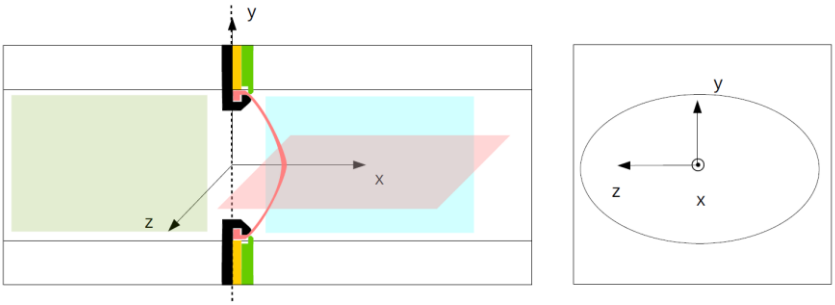

Fig.6: LMFA's referential for PIV and PTV-4D measurements. Source: LMFA's report [1]

The piston was displaced using a crank-rod actuator. Its displacement is close to a sinusoidal movement at a frequency close to 2 Hz. The piston movement is close to a sinus function.

Experimental piston displacement data were fitted by LMFA using a cosine function of the form:

$$A[cos(2(\alpha) + (cod(\beta) - 1)/R] + B$$

Where $\alpha = 2\pi f(t - t_0)$ and $\beta = \arcsin(Rsin(\alpha))$, R being the ratio between the crank and the rod length
Here is the best fit, obtained by LMFA:

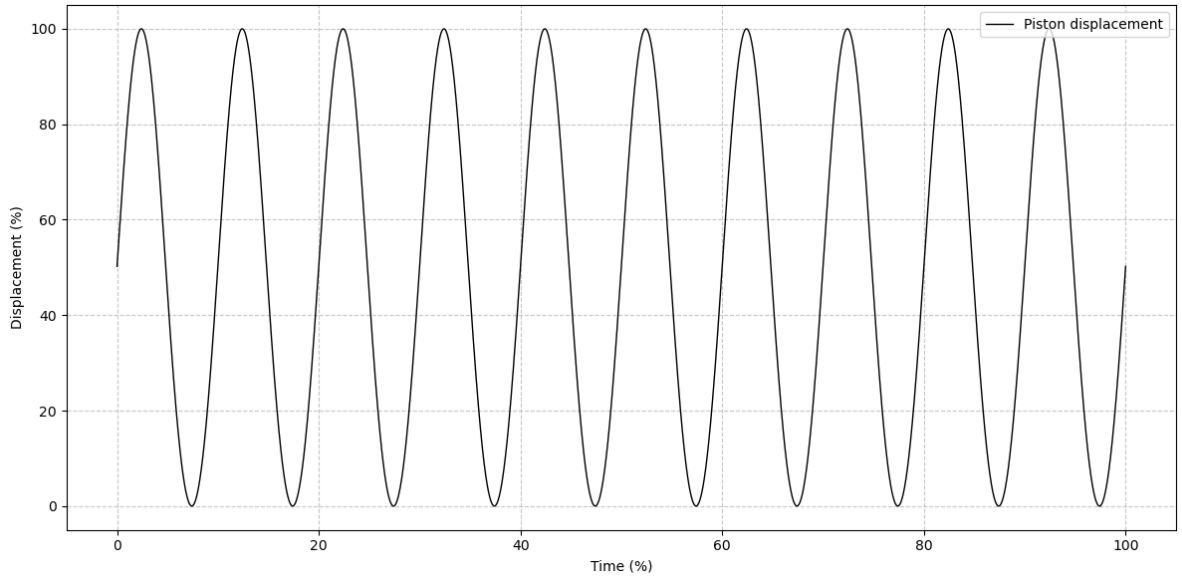

Fig.7: Piston displacement as a function time over 10 cycles.

The membrane is fully retracted at t~0%, t~10% and fully inflated at t~5%, t~15%, etc.

3 Feasibility study: validation of the membrane's hyperelastic behavior

The hyperelastic behavior of the membrane was first validated using LS-DYNA using experimental data from five uniaxial tensile tests conducted by CARMAT on a test specimen taken directly from the hyperelastic membrane:

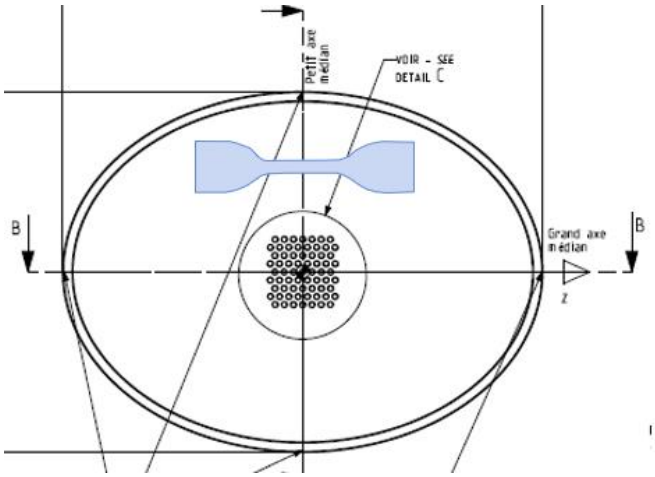

Fig.8: Sampling location of the specimen on the hyperelastic membrane. Source: CARMAT

It was agreed that, for the calibration study, thickness would be considered constant . Since the membrane is primarily subjected to tensile loading during its deformations on the experimental bench, it was also agreed that the assumption of uniaxial tension would be sufficient to adequately approximate its mechanical behavior.

The testing device performed an optical measurement of the displacement between two crosses marked on the specimen:

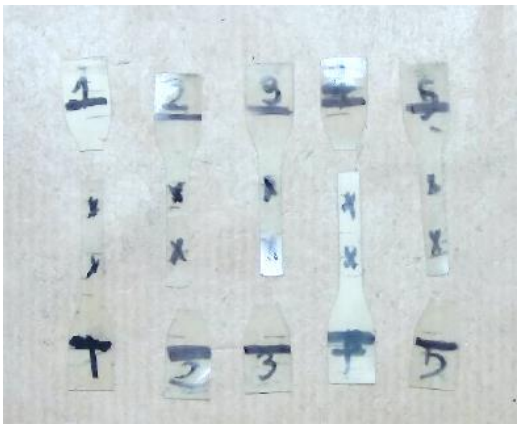

Fig.9: Fracture surface of the test specimens. Source: CARMAT

Only this measured section of the specimen was considered in the modeling. The desired correlation must remain valid up to 200% strain. Only ¼ of the measured gauge section was modeled, with a mesh size of 0.1 mm. The LS-DYNA material model employed for calibration is the "Hyperelastic Rubber" formulation (**`*MAT_077H`**), which provides a general description of hyperelastic behavior, optionally augmented by linear viscoelasticity, as outlined by Christensen [1980]. At the beginning of the computation, Dynas+ used LS-DYNA to generate a set of numerical parameters to perform an initial calibration. This calibration made it possible to determine the six optimized hyperelastic coefficients of the **`*MAT_077`** law. A subsequent sensitivity and optimization phase was carried out using LS-OPT to refine this calibration and reproduce the experimental specimen results. The study conducted by Dynas+, correlated with CAMART's experimental data, successfully reproduced the hyperelastic behavior of the membrane up to 200 % engineering strain:

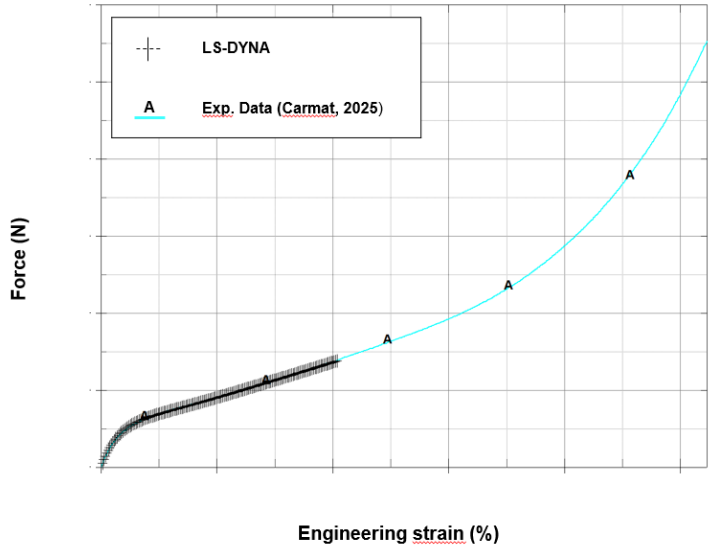

Fig.10: Engineering Force/Strain Curve – Correlation between LS-DYNA Simulation and Experimental Data from five uniaxial tensile tests conducted by CARMAT on a sample of the hyperelastic membrane

The results obtained showed very good agreement between the simulations and the experimental observations, confirming that the working assumptions as well as the numerical parameter choices made in LS-DYNA could be adopted to describe the hyperelastic behavior of the membrane in the FSI simulation.

4 FEM model

4.1 Modeling hypothesis

Only the inner surfaces of the channel, including the tank's inner surfaces and the Membrane have been modelled on DEP Meshworks's pre-processor:

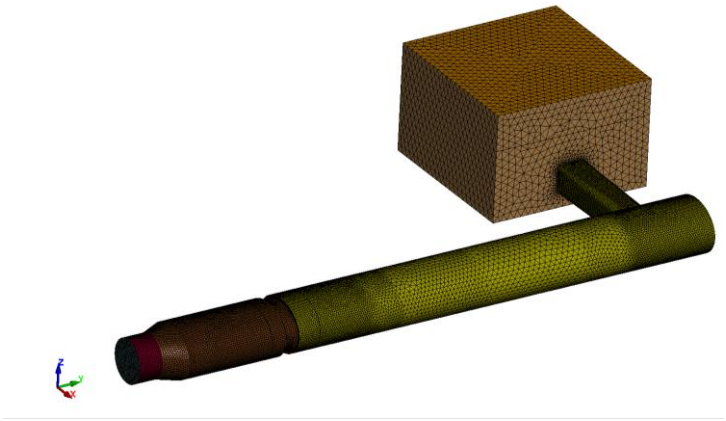

Fig.11: Fluid external surfaces mesh

The Membrane has been modelled with shell elements with a very thin constant thickness. The shape of the center was simplified by creating an extra thickness as a "patch":

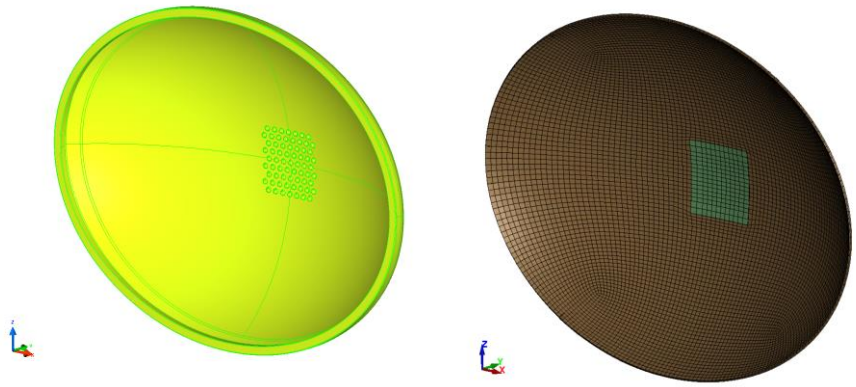

Fig.12: Original geometry of the Membrane (left) and actual modelling (right)

It was simplified using a density-equivalent approach to simulate the mass presence of the microspheres. The objective was to replace the microspheres with an additional thickness equivalent to the volume of the microspheres.

4.2 Materials

The hyperelastic membrane is the only deformable part of the model. The incompressible fluid is modeled with the properties of clear water. Dynas+ also added the internal channel mechanical characteristics to allow LS-DYNA to calculate contacts between the edges and the membrane in case there are any contacts during simulation. The internal channel and the rest of the structure is considered fully rigid which implies that no deformation of the material is possible in the finite elements concerned.

4.3 Mesh

4.3.1 Eulerian elements

Some attention has been given on the mesh size of the fluid domain to ensure precision in complex flow areas like around the piston, around the Membrane and close to the tank:

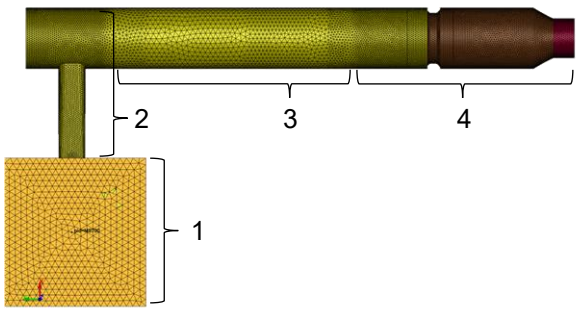

	Average mesh size
1	10mm
2	3mm
3	7.5mm
4	3mm

Table 1: Fluid domain – Average mesh size

4.3.2 Lagrangian elements

The membrane's elements formulation is ELFORM=16 with full integration using four-node thin shell elements, featuring four integration points through the thickness. The average mesh size for the membrane's shells elements is 1 mm. The internal channel is modelled with rigid elements.

4.3.3 Boundary layer meshing

The default method of LS-DYNA, based on mesh size, was used to add five elements in the boundary layer on the walls and on the membrane:

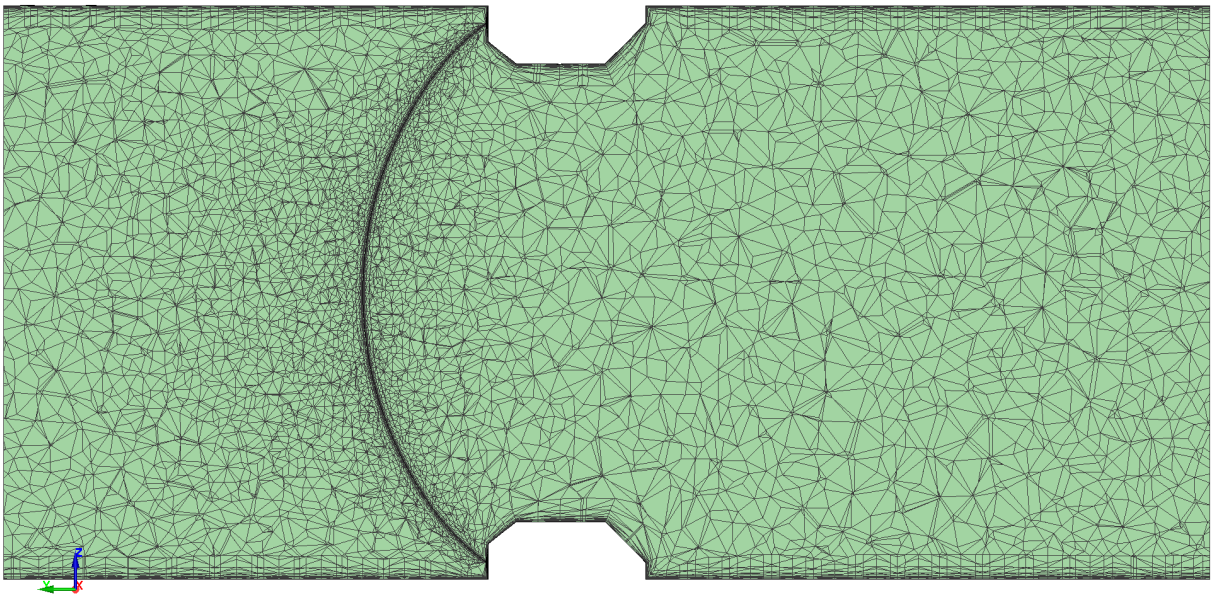

Fig.13: Section cut – Boundary layer mesh

4.4 Boundary conditions

4.4.1 Structure boundary conditions

The membrane's external nodes (marked with red crosses on the edge of Fig.14: below) translations are blocked in every global direction, the rotational degrees of freedom are left free:

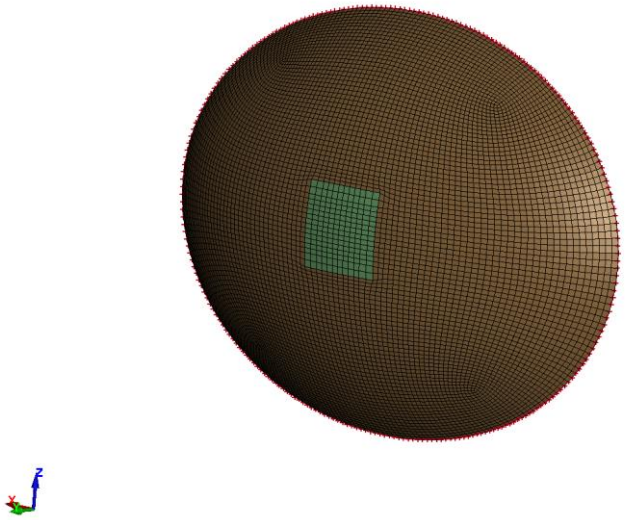

Fig.14: Membrane's boundary conditions

4.4.2 Fluid boundary conditions

A no-slip condition has been defined on every surface including the membrane. It states that at the interface between a viscous fluid and a solid boundary, the fluid velocity matches the velocity of the boundary. In practical terms, if the solid surface is stationary, the fluid in direct contact with the surface also has zero velocity relative to that surface. This condition is mandatory to accurately model velocity gradients from the walls, as it reflects the physical reality that fluid particles adhere to the boundary due to molecular interactions. The initial fluid volume was initialized using the levelset technology with an initial height:

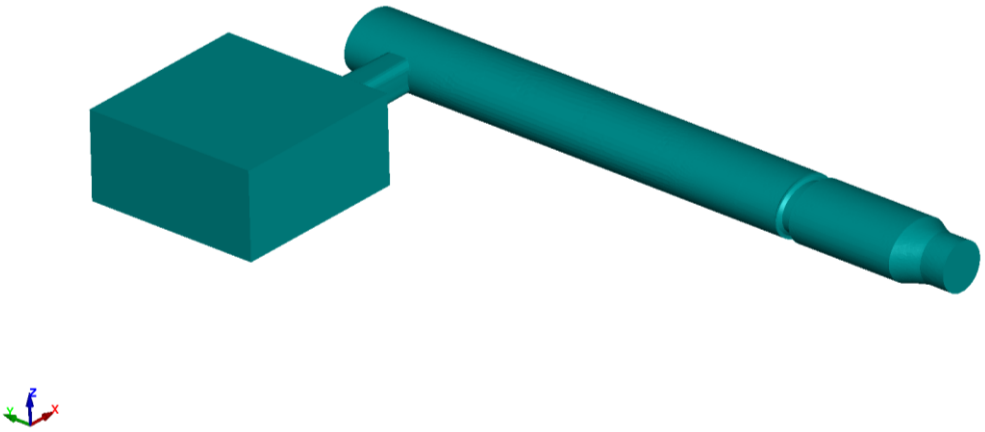

Fig.15: Initial level of water inside the test bench

4.5 Load case

The test case consists in reproducing the movements of the piston located upstream. We used a technique that's consists of meshing the internal surface of the piston and impose a mesh movement following the $\vec{x}$ axis.

Fig.16: Piston modeling: mesh motion

The real displacement of the piston was added to the model through mesh motion using **`*ICFD_BOUNDARY_PRESCRIBED_MOVEMESH`** LS-DYNA keyword.

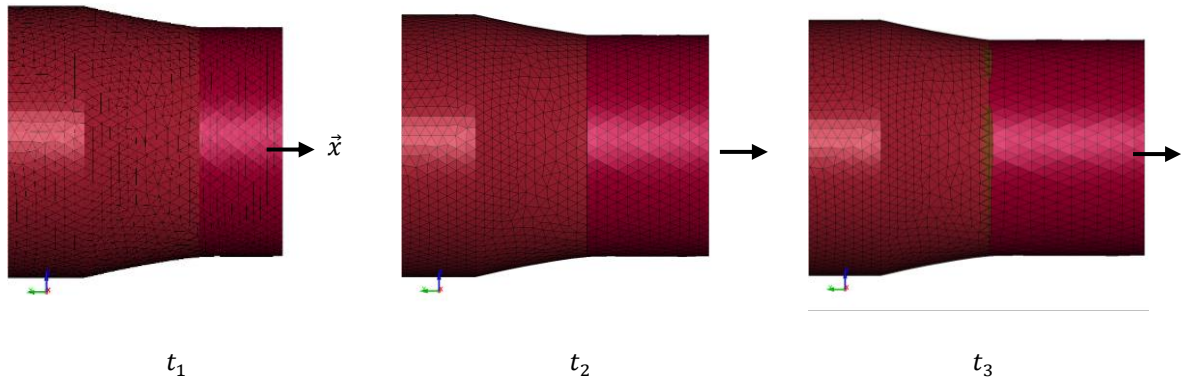

Fig.17: Piston's displacement – mesh motion at different time

The original position of the mesh is at time t_2 in this example. At t_1, the mesh is compressed to simulate the displacement following $+\vec{y}$ and at t_3, the mesh is extended to simulate the displacement following $-\vec{y}$.

5 Fluid-structure coupling

In LS-DYNA, the detection of the coupled structure is done by searching for nodal proximity between the fluid surfaces declared coupled and any structural element. Since weak coupling tends to provoke instabilities, strong coupling will always be the best choice considering both solvers are iterating to reach convergence. These calculations have therefore been conducted with a strong integration scheme.

6 Post-processing methods

To correlate with experimental results, we used **`*ICFD_DATABASE_POINTOUT`** LS-DYNA keyword to extract, at precise locations, the velocities in every direction. The method used to calculate the fluid velocities in the experiment is called Particle Image Velocimetry (PIV):

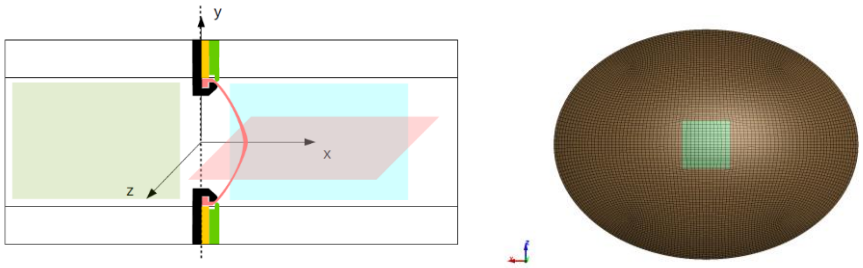

Fig.18: LMFA's laser sheets (left), CAD of the Membrane and global CAD reference (right)

Because the two referential differ and, to compare the same points as those used by the PIV method to obtain the velocity fields on the same areas, the following transposition was carried out:

$$\begin{aligned}\overrightarrow{x_{LMFA}} &= \overrightarrow{y_{CAD}} \\ \overrightarrow{y_{LMFA}} &= \overrightarrow{z_{CAD}} \\ \overrightarrow{z_{LMFA}} &= \overrightarrow{x_{CAD}}\end{aligned}$$

Rotation naturally applies to other potential variables (displacements, velocities, accelerations). This transposition allowed us to create the same planes to extract the velocity fields:

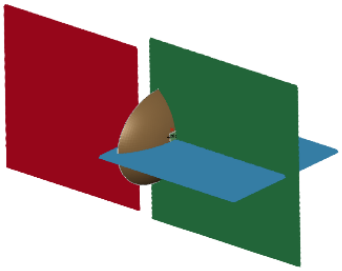

Fig.19: Visualization of the numerical "laser sheets" (colors do not match Fig.18:)

All results will thus be presented using the CAD reference.

7 Results

7.1 PTV analysis

The comparison between the displacement of the structural part only is presented below for three states: fully deflated (beginning of a cycle), fully inflated and fully deflated (end of a cycle). Nodal positions have been extracted from the simulation and the experiment. The same Python script allowed to 3D plot nodal positions in an interactive HTML window. The results presented below are showing the maximum deformation of the membrane over the last cycle. The table below shows the membrane's deformation on those three states:

	PTV – Experiment	PTV – LS-DYNA simulation
Fully deflated (beginning of a cycle)	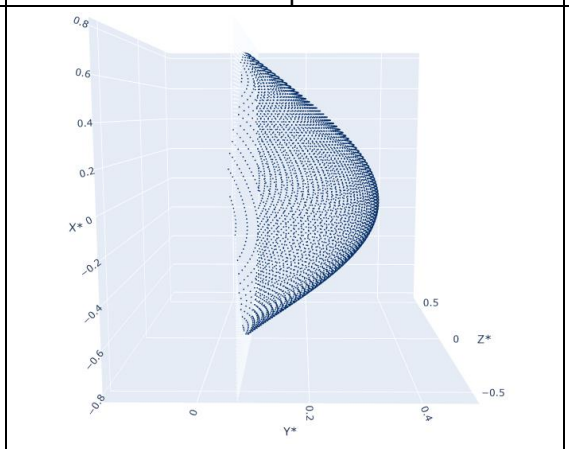	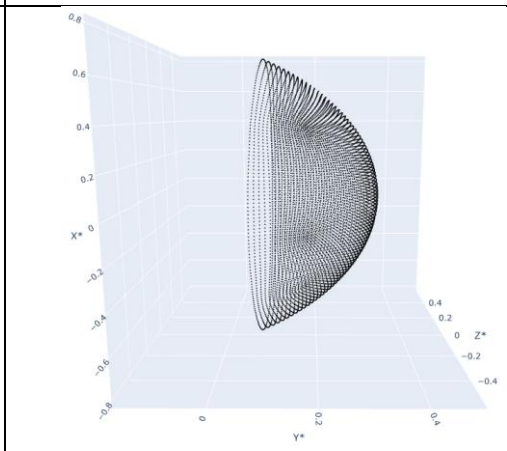
Fully inflated	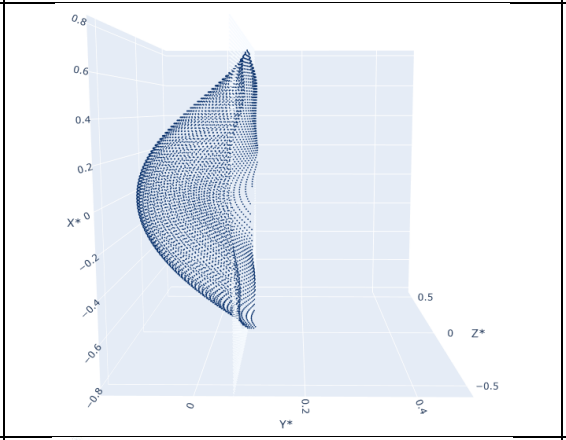	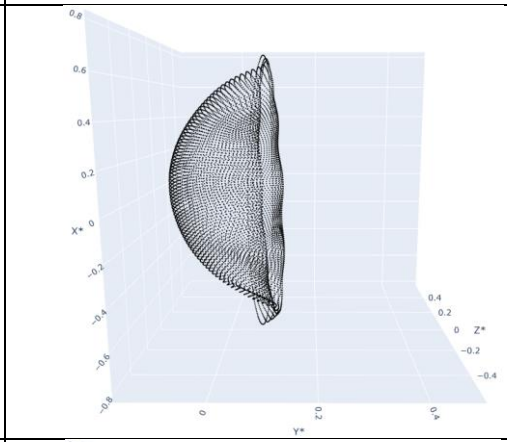
Fully deflated (end of a cycle)	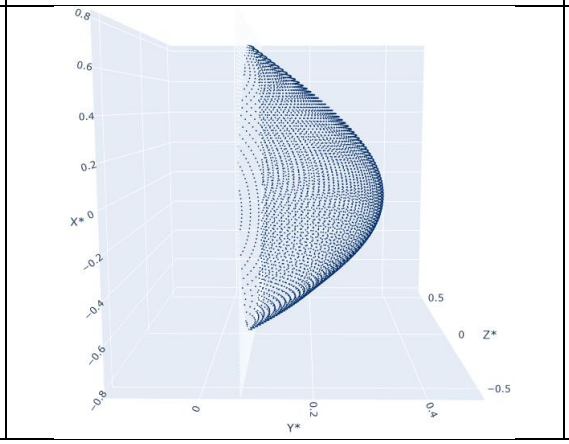	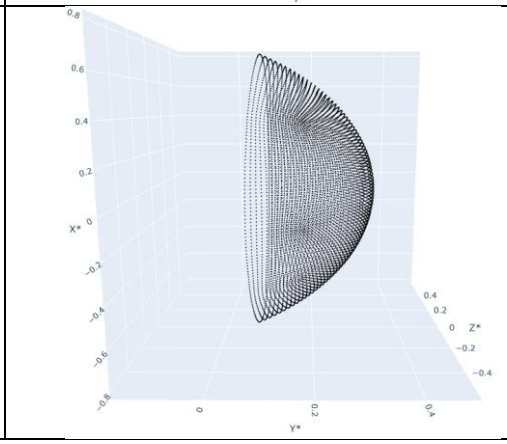

All spatial quantities in this study were non-dimensionalized using the smallest radius of the membrane, while the velocities were normalized with respect to the experimentally measured minimum and maximum values.

The mechanical behaviour of the membrane is well reproduced except for the maximum deformation levels. In the experiment, the membrane is deforming approximately 5% more than in the LS-DYNA simulation. We can observe that the edges are not fully sucked to the other side. It is mainly due to the boundary conditions that are not very representative of the real fixation system supposed to pinch the membrane on its far extremities which were cut in the finite element model. This could also explain why the membrane in the simulation is lacking flexibility.

To ensure that the flow is well established, 10 cycles have been run:

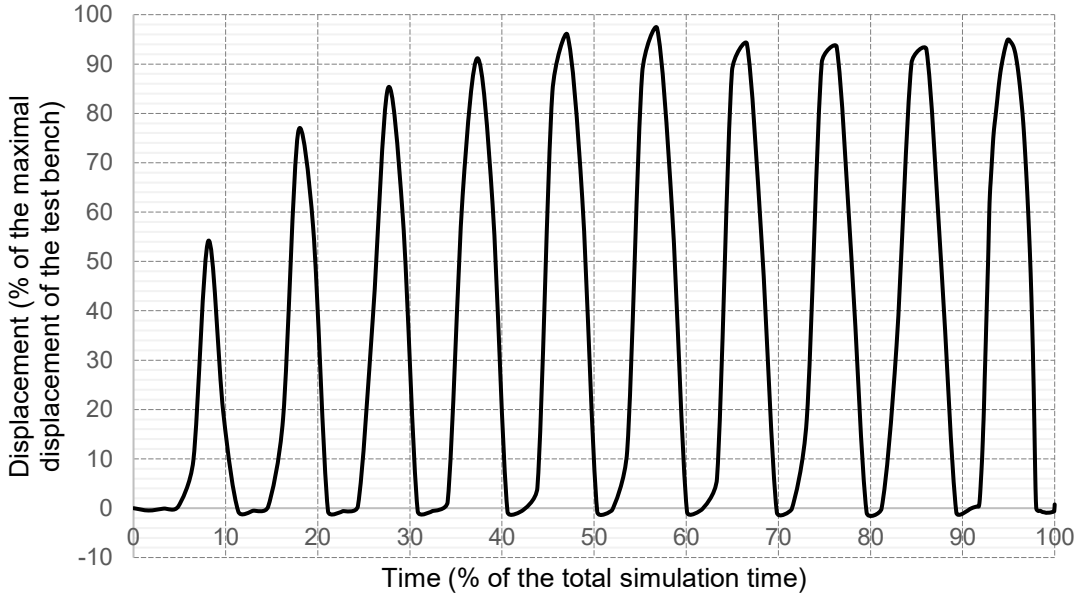

Fig.20: Y displacement of the central node of the membrane during the whole simulation time

This graph shows the importance of letting the simulation stabilize to avoid transient effect and reach an almost stationary or pseudo-periodic state in this case. The initial cycles often contain transient effects that are not representative of the long-term or established behaviour of a system. Here are a few possible reasons. At the beginning of the simulations, the initial conditions are generally non-physical: the velocity field is often set to zero or only roughly estimated, the level set interface may not be correctly shaped or positioned, and the pressure field is typically not in equilibrium, which induces artificial pressure waves. In a closed duct, such waves reflect off the walls and may generate oscillations that require time to dampen or stabilize, particularly in the incompressible regime. In addition, the level set function itself needs time to stabilize and to properly advect with the flow, and the first piston motions can distort the interface before it fully adapts to the dynamics. Finally, the piston-induced motion generates shear and vortical structures in the fluid, which usually require several cycles to evolve into a regular and periodic pattern.

Nevertheless, results are very close to the test bench data and showcase LS-DYNA abilities to represent such FSI behaviours.

7.2 PIV analysis – Upward – Vertical plane

The comparison between the displacement of the structural part only is presented below for three states due to the amount of data gathered. Each graph displays a velocity-coloured map with velocity vectors. For example, on a $(i\ ,\ j)$ map, the vectors are calculated like the following: $\vec{v} = V_i \cdot \vec{\imath} + V_j \cdot \vec{\jmath}$ with V_i, V_j being the velocity values in each direction of the plan.

7.2.1 Horizontal component

These three states represent the undisturbed flow over the cycle and the peak velocity fields in the vertical and horizontal directions on the plane of interest.

Table 2: Velocity fields – Upward – Horizontal component (Vertical plane)

Time	LMFA's test bench	LS-DYNA simulation
t_0	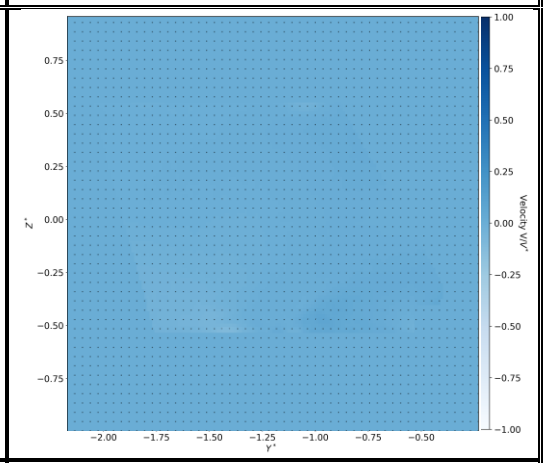	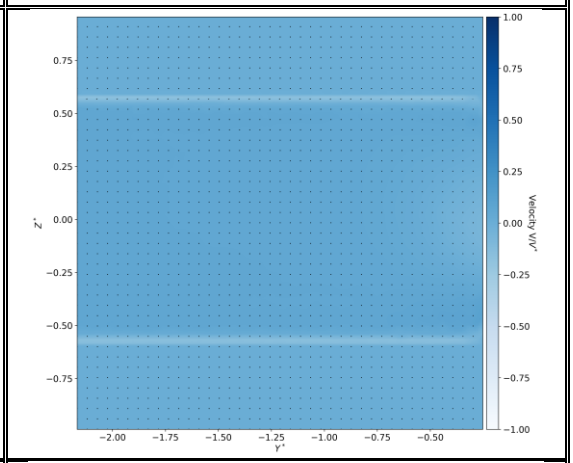
t_1	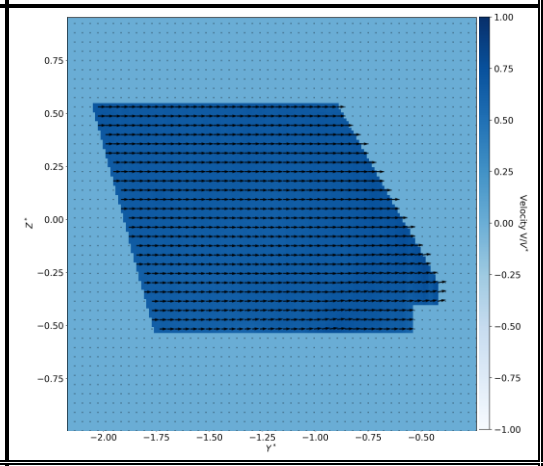	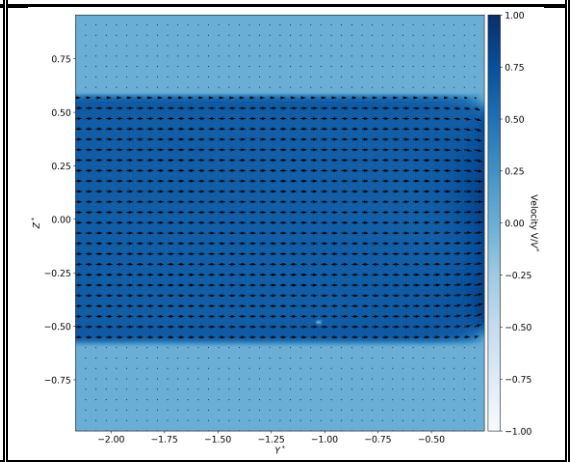
t_2	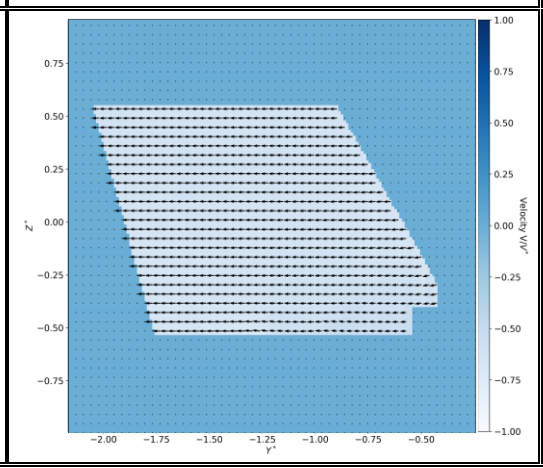	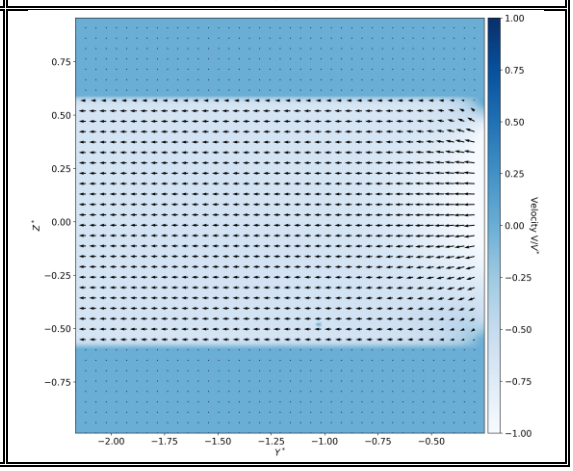

7.2.2 Vertical component

Table 3: Velocity fields – Upward – Vertical component (Vertical plane)

Time	LMFA's test bench	LS-DYNA simulation
t_0	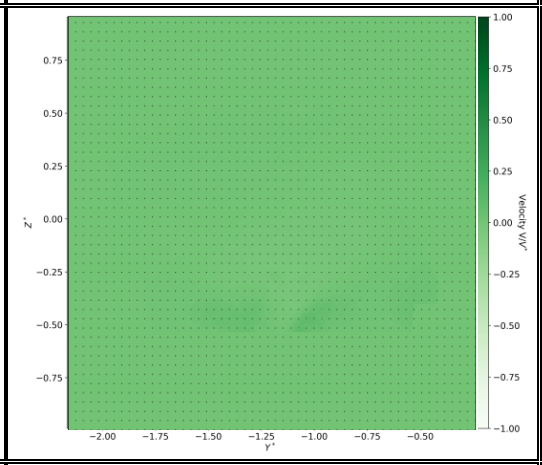	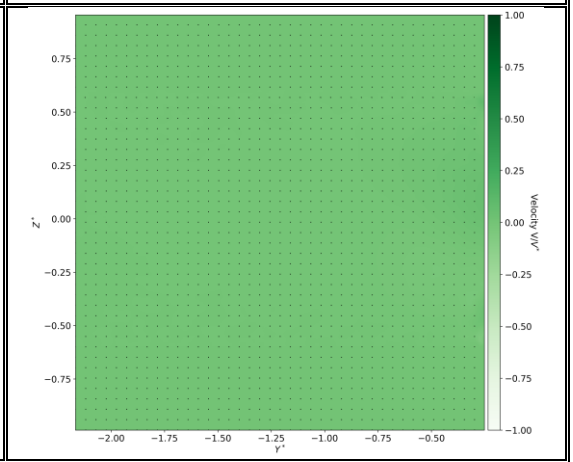
t_1	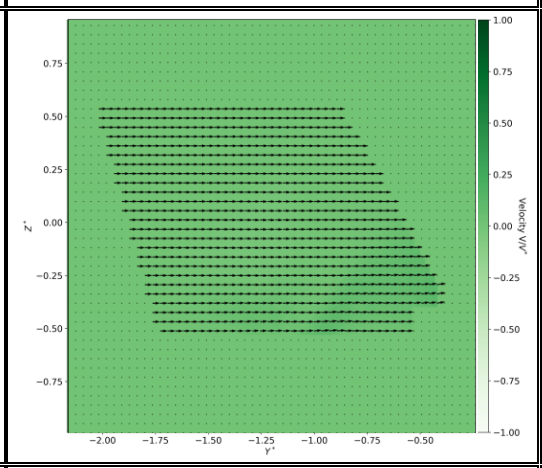	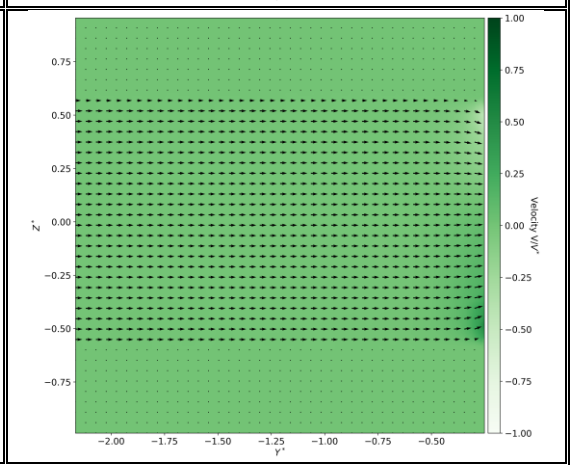
t_2	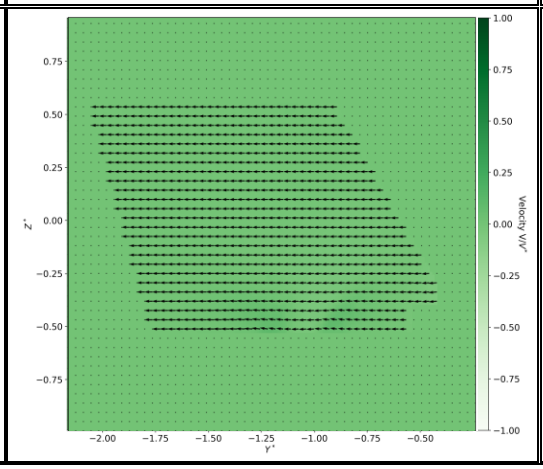	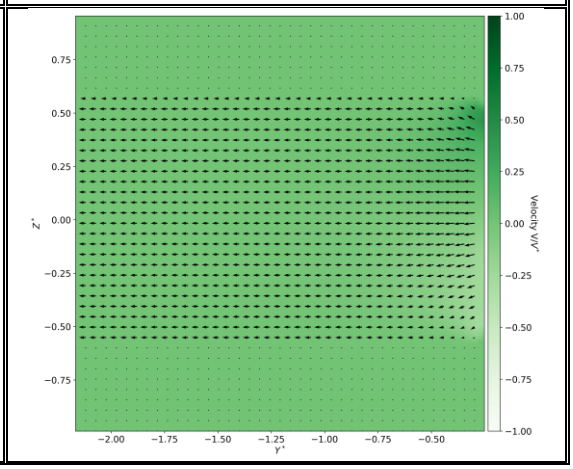

7.2.3 Discussions

The LS-DYNA simulation fits well to experiment results. Since there are more points for analysis on LS-DYNA, the size of the vectors may be influenced by the flow on the other side of the ventricle and may not correspond exactly to the upward zone. That explains the small differences regarding vectors. On the other hand, the colormap is very alike.

7.3 PIV analysis – Downward – Horizontal plane

Unlike the precedent section, the three states presented below show transient phases where the membrane moves during a cycle.

7.3.1 Horizontal component

Table 4: Velocity fields – Downward – Horizontal component (Horizontal plane)

Time	LMFA's test bench	LS-DYNA simulation
t_0	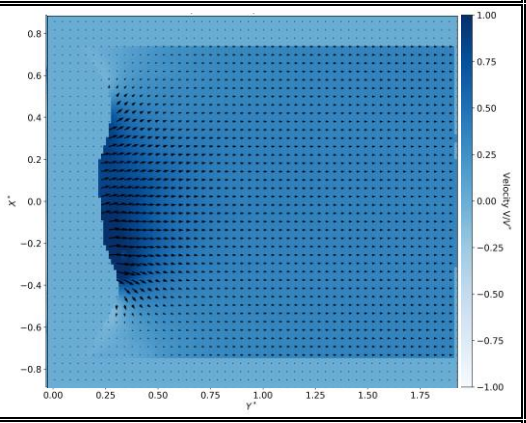	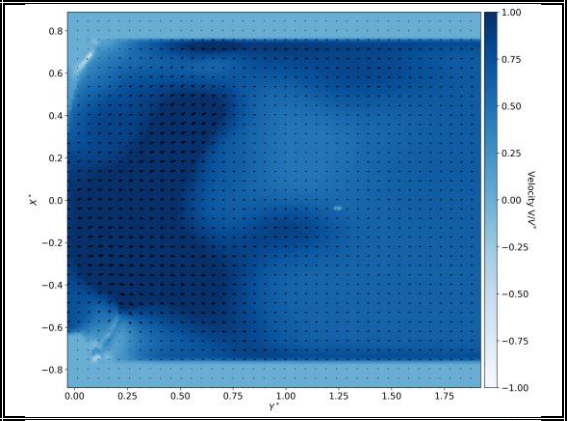
t_1	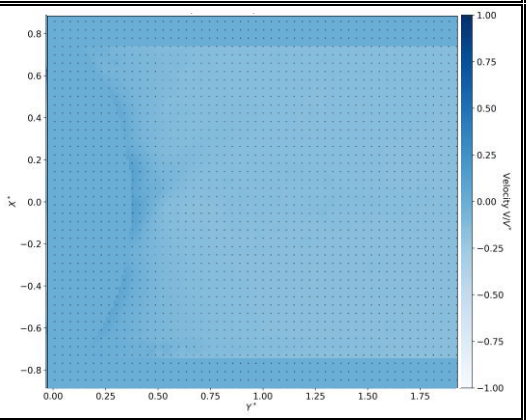	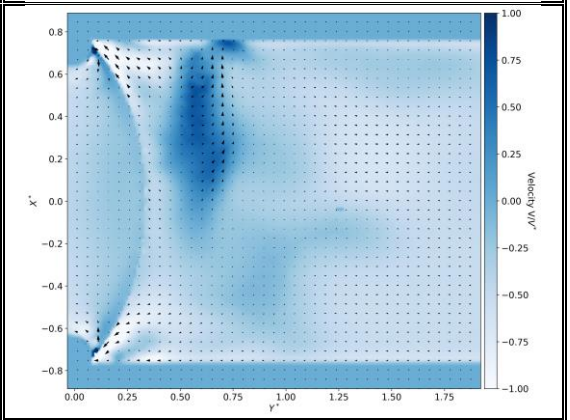
t_2	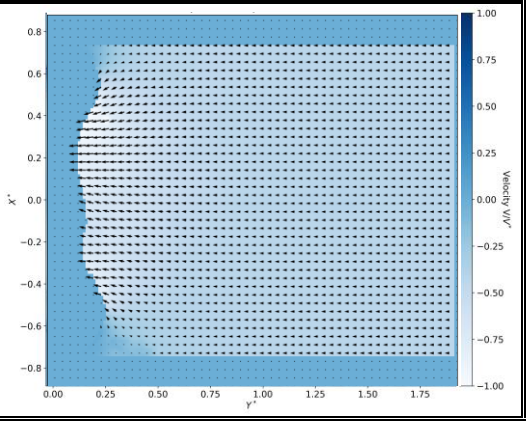	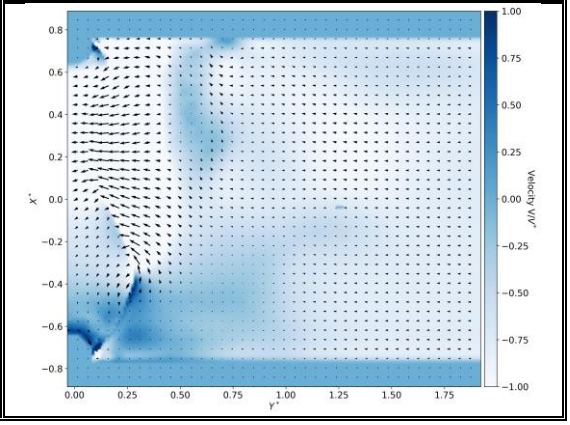

7.3.2 Vertical component

Table 5: Velocity fields – Downward – Vertical component (Horizontal plane)

Time	LMFA's test bench	LS-DYNA simulation
t_0	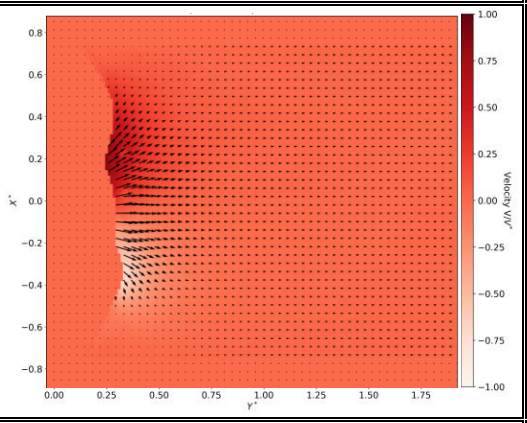	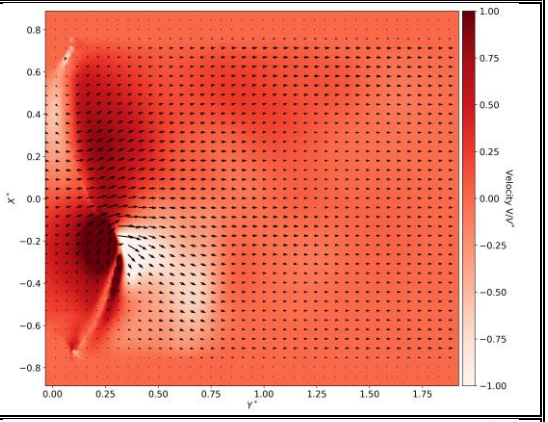
t_1	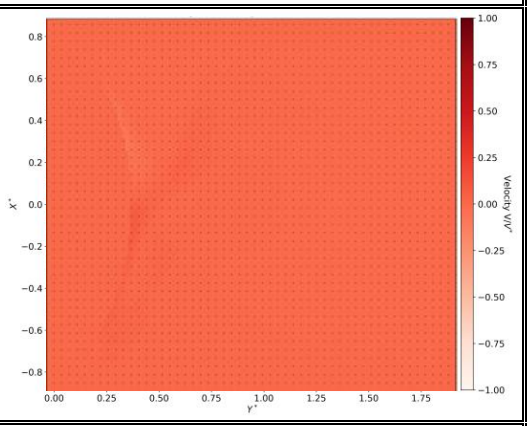	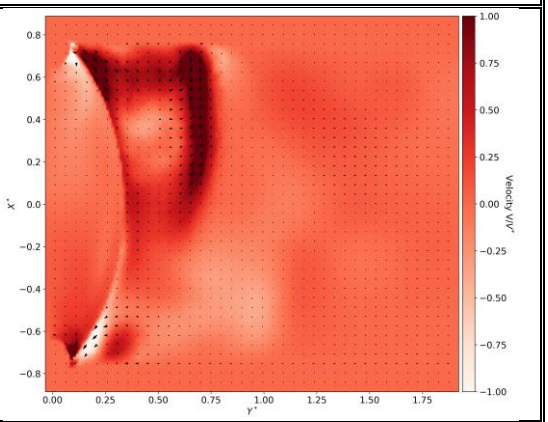
t_2	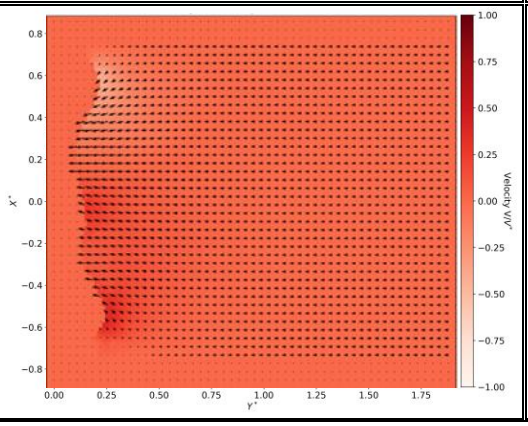	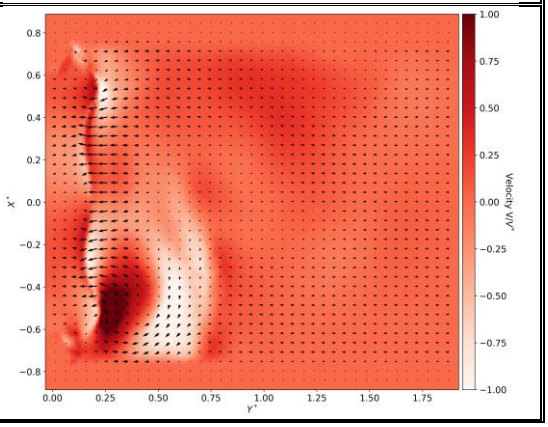

7.3.3 Discussions

Both LS-DYNA and experiment results colormaps are similar with some differences in the maximum velocities values and fluid behaviour. There is a small delay in the fluid dynamic response sequence between both results and once again, vectors sized in LS-DYNA results are influenced by the flow on one side of the ventricle so if the flow has more speed, then the vectors arrows will be smaller on the other side. The flow is recirculating more in the simulation; eddies are better captured than in the experiment but tend to dissipate slower.

7.4 PIV analysis – Downward – Vertical plane

Unlike the precedent sections, the three states presented below show transient phases where the membrane moves during a cycle.

7.4.1 Horizontal component

Table 6: Velocity fields – Downward – Horizontal component (Vertical plane)

Time	LMFA's test bench	LS-DYNA simulation
t_0	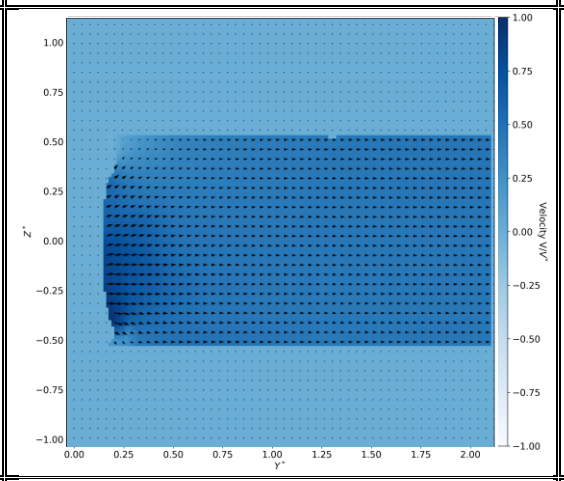	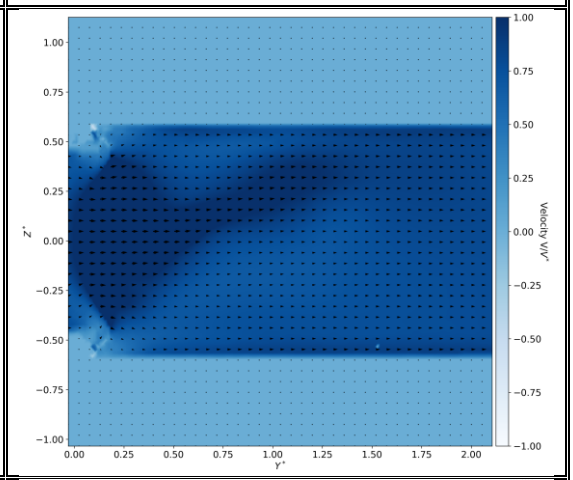
t_1	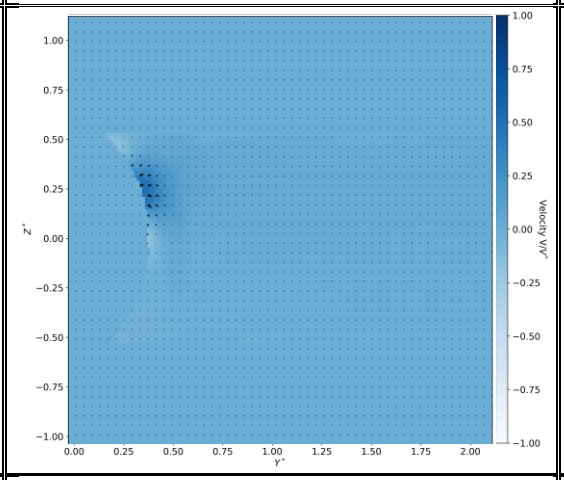	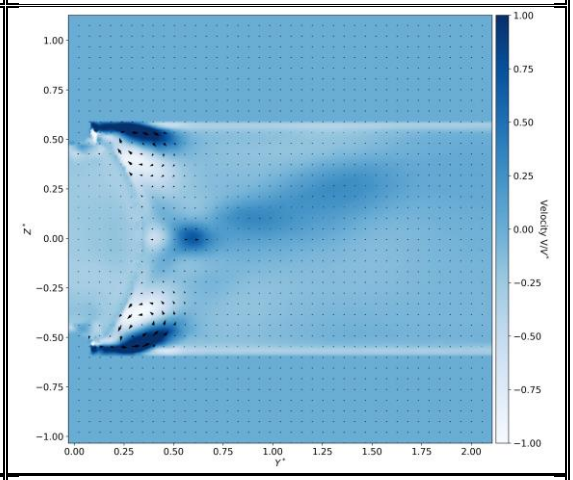
t_2	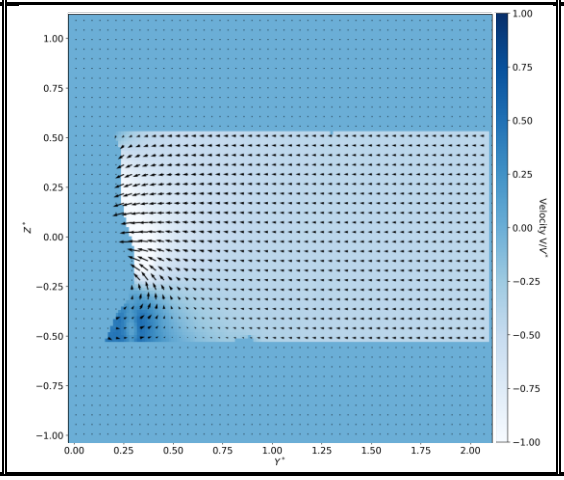	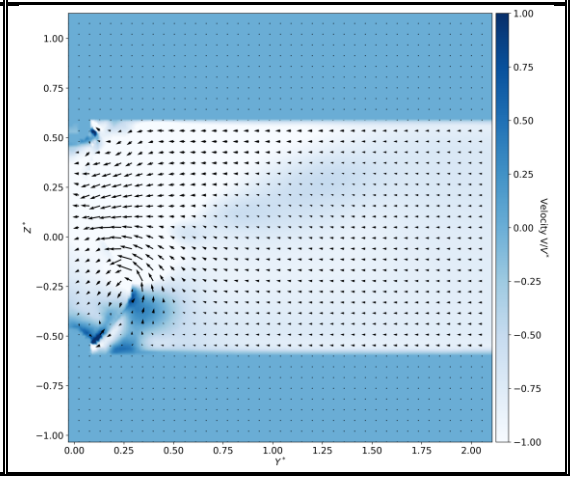

7.4.2 Vertical component

Table 7: Velocity fields – Downward – Vertical component (Vertical plane)

Time	LMFA's test bench	LS-DYNA simulation
t_0	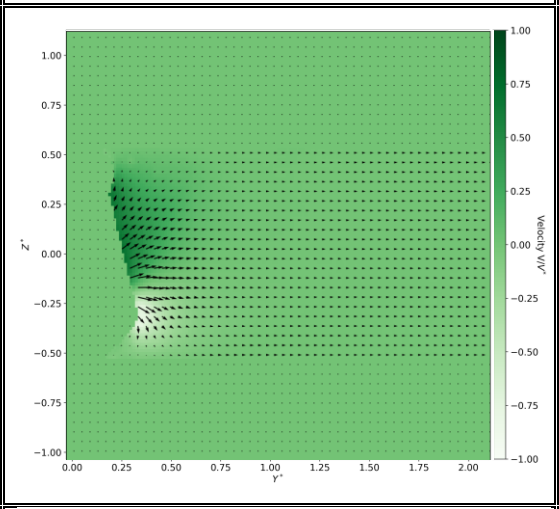	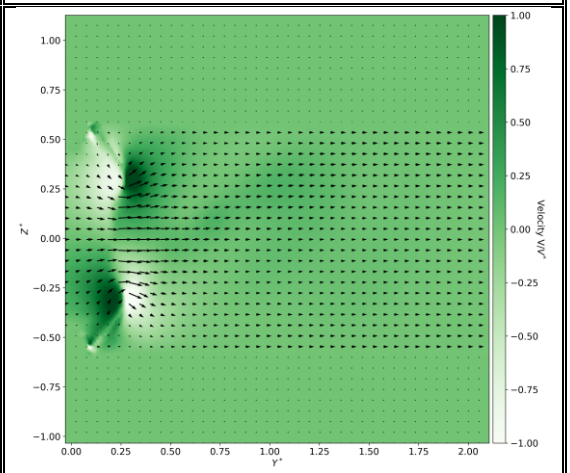
t_1	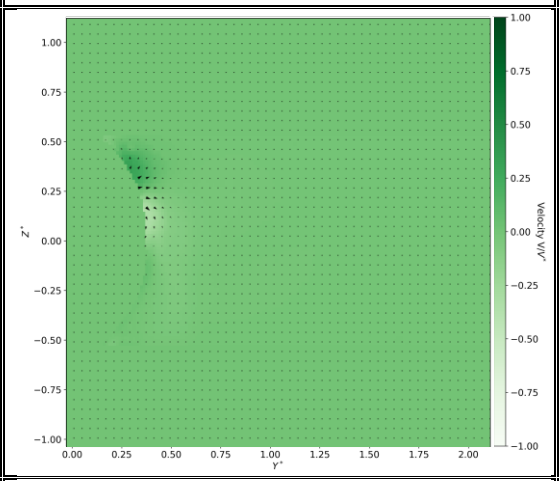	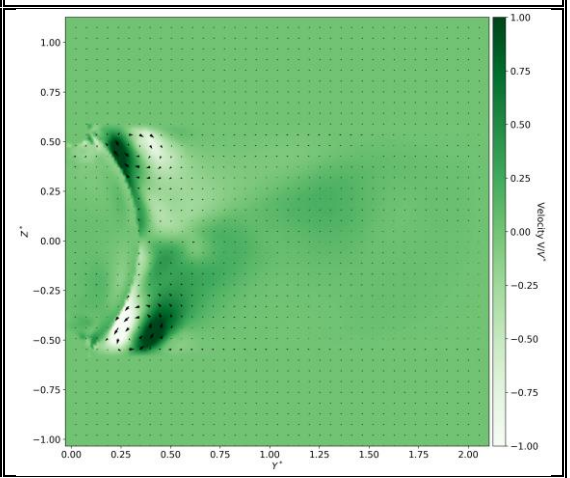
t_2	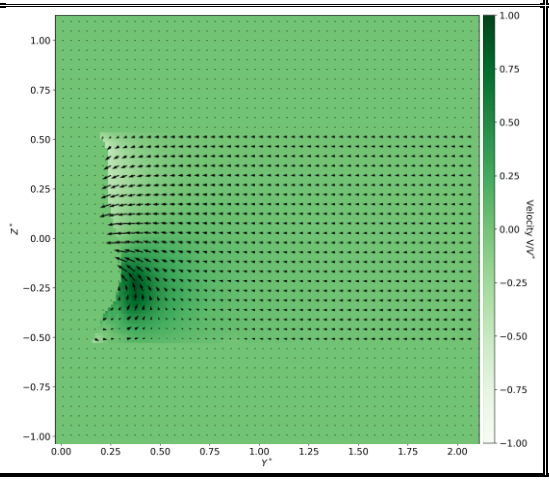	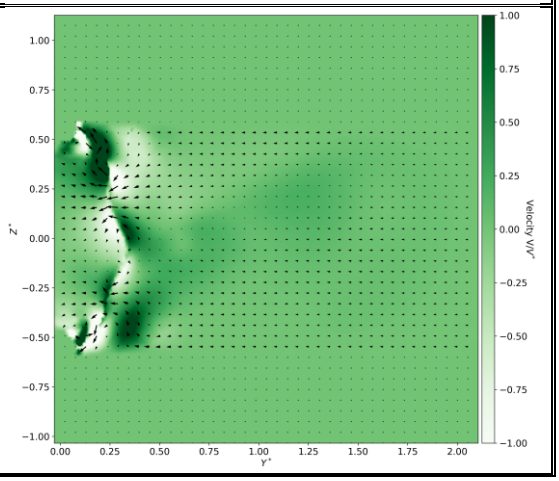

7.4.3 Discussions

We can also observe a delay in the deformation sequence with this comparison. In the simulation, small recirculation of the fluid can be observed. The global behaviour is pretty good, and the eddies may be a direct consequence of the turbulence model choice.

8 Conclusion

This study aimed to reproduce an experimental bench test to validate the behaviour of an hyperelastic membrane immersed in a water flow channel controlled by a piston. To do this, the water channel and the tank with the right level of water have been modelled. The simulation was conducted over 10 cycles to ensure that the flow is established, and the transient effects are avoided. The PIV analysis was compared with LS-DYNA simulation results through three significative states depending on the side of the membrane. The global fluid behaviour is matching the experimental data well with small differences like little eddies formations and maximum local velocities differences. It appears that LS-DYNA is capturing more information regarding the vorticity zones downward the membrane than in experiments. Velocity colourmaps are, nevertheless, showing a strong similarity in velocity levels.

It also appears that, in the PIV numerical results, the downward flow is behaving with a small delay compared to the experiment for all cycles while the deformation of the membrane seems to follow well the timescales. This could be due to the tank's boundary conditions, the modelling hypothesis of the membrane's edges and the turbulence model choice. It could also be due to the absence of the sights at the center of the membrane which could act, in the experiment, as turbulence reducers. The small vortices observed may be due to two main reasons. First, the turbulence was modelled with the ICFD default, a residual-based Variational Multiscale (VMS) stabilization. It does not explicitly compute each eddy scale; instead, it models the effect of unresolved scales through numerical dissipation. Depending on the objectives and mesh resolution, an explicit LES subgrid model may provide better control of small-scale dissipation on a moderately refined mesh, provided the grid and time step satisfy basic LES resolution requirements. In this study, turbulence was modeled with the default residual-based Variational Multiscale (VMS) scheme in the ICFD module of LS-DYNA. VMS provides robustness and efficiency, as it stabilizes solutions on relatively coarse meshes without strict resolution requirements, making it well suited for capturing global flow behavior. Its implicit treatment of unresolved scales through subgrid dissipation, however, can limit accuracy when fine turbulent features or detailed experimental comparisons are required. Explicit Large Eddy Simulation (LES) models, such as Smagorinsky or WALE demand finer meshes and smaller time steps, increasing computational cost by great factors. The choice between VMS and LES therefore depends on the balance between available resources and the required level of turbulence detail.

Secondly, the speed discontinuity coming from the membrane's corners is coming from a "triple point" shown below:

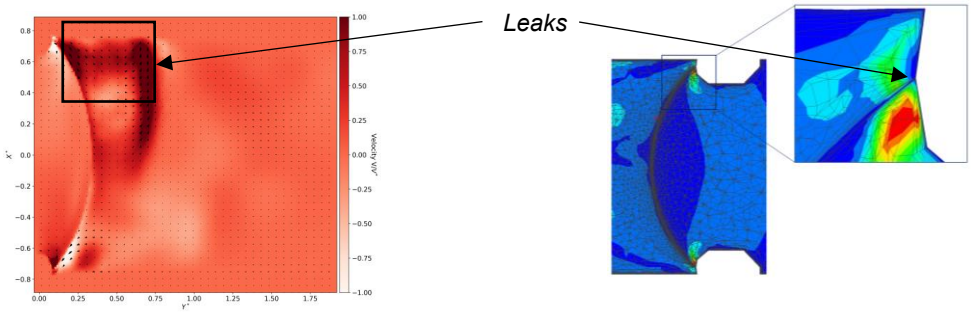

The Eulerian membrane is represented by an LS-DYNA technology called *MESH_EMBEDSHELL which is mandatory to allow the fluid solver to consider the thickness of a part modelled with shells. The PTV analysis was compared with LS-DYNA simulation results between the three same states than for the PIV analysis. The ventricle's mechanical behaviour is also matching well the experimental data with small differences in the deformation sequence. The non-symmetrical behaviour of the hyperelastic membrane is also captured. The edge's movement of the membrane is not fully reproducing the experimental data by not deforming as much as in the experiment. The maximum membrane deformation is reaching approximately 95% of the maximum deformation in the experiment. This discrepancy may stem from the limited number of simulated cycles, or alternatively from the meshing of the ventricle. Modelling hypothesis like the constrained edges of the membrane could also participate in the differences observed.

The results presented confirm LS-DYNA capabilities in reproducing the fluid and mechanical global behaviours of the experimental test bench of the membrane conducted by LMFA with small differences probably due to modelling choices.

9 Summary

The study demonstrates LS-DYNA capacities to reproduce with good accuracy the experimental bench test of a hyperelastic membrane immersed in a piston-driven water channel conducted by LMFA under CARMAT authority. The global fluid behavior predicted thanks to the simulation matches well with PIV measurements, with small differences such as the formation of local eddies and slight variations in maximum velocities. LS-DYNA appears to capture more detail in the vorticity zones downstream of the membrane compared to the experiments, while the velocity maps from both approaches show strong overall agreement. A minor delay was observed in the downward flow in the numerical results, which could be linked to boundary conditions, assumptions on membrane edge constraints, turbulence modelling, or the absence in the simulation of experimental elements acting as turbulence reducers. The turbulence was treated with the default residual-based Variational Multiscale method, which may explain the persistence of small vortices, and the membrane's corners introduced additional flow discontinuities. On the structural side, the deformation and non-symmetrical behavior of the membrane are well reproduced, with the maximum deformation reaching approximately ninety-five percent of the experimental value. Differences remain in the deformation sequence and edge movements, which may be attributed to the meshing strategy, the limited number of simulated cycles, and the modelling assumptions. Overall, the results confirm LS-DYNA's ability to capture both the fluid and structural behavior of the membrane test bench, with the observed discrepancies largely explained by modelling choices rather than fundamental limitations of the solver.

10 Literature

[1] CNRS, Ecole Centrale de Lyon, INSA Lyon, Universite Claude Bernard Lyon 1, LMFA, UMR5509, 36 Avenue Guy de Collongue 69134 Ecully Cedex : "*Experimental study of the flow downstram of the hybrid membrane of an artificial heart*", February 2025, p.1-7

[2] Ansys Inc. Southpointe 2600 Ansys Drive, Canonsburg, PA 15317: "*Ansys LS-DYNA Keyword user's manuel Vol. I, II, III*", LS-DYNA R15